İSTANBUL UNIVERSITY CERRAHPAŞA

ORIGINAL ARTICLE
Electrica 2022; 22(1): 7-15

Additional Pulses in the Time Response of a Modal Filter on a Double-Sided Printed Circuit Board

Maria A. Samoylichenko, Talgat R. Gazizov

Department of Television and Control, Tomsk State University of Control Systems and Radioelectronics, Tomsk, Russian Federation

Cite this article as: M. A. Samoylichenko and T. R. Gazizov, "Additional pulses in the time response of a modal filter on a double-sided printed circuit board," *Electrica*, 22(1), 7-15, Jan. 2022.

ABSTRACT

A quasistatic approach was used to consider the occurrence of additional pulses (APs) in the modal filter (MF) realized on a double-sided printed circuit board, as well as in the three structures obtained from it by removing one reference conductor. It is shown that, for all investigated MFs, the AP delays are determined by a linear combination of per-unit-length mode delays multiplied by the line length. It was found that there are no APs between the pulses of modes with one pass along the line, while they appear with three or more passes. It is revealed that in each of the considered MF structures (except the one without upper-right reference conductor), the APs have greater amplitudes of mode pulses with a triple pass. It was demonstrated that the removal of the reference conductors affects the number, polarity, and amplitude of the APs.

***Index Terms*—**Additional pulses, double-sided printed circuit board, modal filter, protection device, reference conductor, ultrashort pulse.

I. INTRODUCTION

Ensuring electromagnetic compatibility is relevant because the scope of modern electronic equipment is constantly growing. In real operating conditions, the quality of electronic equipment operation is frequently reduced under the influence of electromagnetic interference (EMI). Nanosecond and subnanosecond pulses, called ultrashort pulses (USPs), are especially dangerous [1-3]. A USP is dangerous because of its large amplitude, high penetration ability, and large energy [4]. Reduced USP amplitude and energy distribution pose a lower danger to equipment compared to the original interfering signal. Therefore, the problem of protecting equipment against electromagnetic interference (EMI) is urgent.

Among the wealth of protective devices, there are three most widely-used types: discharge, semiconductor, and vacuum [5,6]. However, they all have some disadvantages. The main disadvantage of gas-discharge protectors is the low speed of operation. Semiconductor protection devices have two significant disadvantages. Firstly, in any combination of the integrated protective diodes, the failure of one leads to an uneven distribution of the absorbed power of the other diodes. This leads to an avalanche of destruction of the entire protective device. Second, the disadvantage inherent to all types of semiconductor limiters is large inter-electrode capacitance that limits their use in high-frequency circuits. The disadvantages of vacuum-protective devices include band-limitedness, resonator heating, and the difficulty in maintaining secondary emission at a high current density. In addition, widespread protective devices such as EMI filters are not able to properly protect against USPs [3,5,7,8]. Thus, despite the variety of methods and means of protection from the effects of powerful EMI, the problem of effective protection has not yet been solved.

A relatively new method of protection from EMI is the decomposition of large-amplitude pulse into a series of lower-amplitude pulses. This is achieved through the "beneficial" use of mutual couplings in transmission lines with non-homogeneous dielectric filling. This method is used in modal filters (MF) and can be realized both in power supply circuits and in data transmission systems [9-11].

Corresponding Author:
Maria A. Samoylichenko

E-mail:
1993mary2011@mail.ru

Received: July 9, 2021

Revised: October 12, 2021

Accepted: November 8, 2021

DOI: 10.5152/electrica.2021.21079

II. PROBLEM STATEMENT

In [12], the occurrence of additional pulses is shown in the example of the structures with modal redundancy, reflection-symmetric meander lines, MFs with a passive conductor in the cut of the reference plane, and meander delay lines with a broad-side coupling. Thanks to these pulses, it is possible to further distribute the energy of a dangerous USP over time, and, in some cases, to minimize the maximums of the mode pulse amplitudes. Since USP attenuation is estimated precisely by the maximum of the pulse amplitudes at the MF output, this point is significant.

It is shown that the delays of the APs can coincide both with each other and with the main pulses, resulting in an increase in the total amplitude. The delays of such pulses are determined by various linear combinations of the per-unit-length delays of the line modes. The presence of APs has been experimentally proven. Therefore, the study of APs in the MF and the identification of their possible combinations are highly relevant.

In [13], the effect of removing one or two reference conductors in the MF on a double-sided PCB was considered in order to reduce the mass. However, a detailed study of this work showed the presence of APs. Therefore, it is useful to investigate them in more detail. The purpose of this work is to study the APs, and their combinations in the MF implemented on a double-sided printed circuit board and in the structures obtained from it by removing one reference conductor.

III. SIMULATION APPROACH

While formulating the problem and taking into account the available data and the accuracy requirements, it is necessary to determine which approach will be used: circuit analysis, quasistatic, or electrodynamic approaches. In their frameworks, one could distinguish heuristic, analytical, numerical, and combined methods. The circuit analysis approach is based on Kirchhoff's laws and the simulation is performed using circuit diagrams. The electrodynamic approach based on the solution of Maxwell's equations is universal and allows solving the problems with arbitrary geometry. However, when using this approach, the computational resource requirements can be extremely high. An intermediate position is occupied by a quasistatic approach based on the fact that the transverse dimensions of the system are much smaller than the wavelength of signals propagating in it. This allows us to consider the presence of only the main TEM waves without considering the waves of the higher type. The field distributions are calculated from electrostatic and magnetostatic problems requiring the Poisson–Laplace equation to be solved. This approach has become widespread in simulating transmission lines by using telegraph equations and their derivatives.

The quasistatic approach is implemented in the TALGAT software, validated in [14]. The system is based on mathematical models based on the method of moments, where almost all calculations are reduced to matrix operations. One of the features of the software is the ability to set a large number of parameters to allow for various research. For example, one can simulate coaxial, microstrip, strip, coplanar transmission lines, etc. In the quasistatic approach, the electrical characteristics of multiconductor transmission lines are described by matrices of the per-unit-length parameters—R (Ω/m), L (H/m), C (F/m), and G (S/m).

In [14], the simulation results obtained with different methods are compared (Green's function method (GFM), method of moments (MoM), and variational method (VM)). It is shown that the results of MoM implemented in the TALGAT software are in good agreement with other numerical methods. For two coupled strips on a substrate, the values of matrices L and C obtained in the TALGAT software and given in [15] are compared. Cases in which the side dielectric walls become closer to the side edges of the strips, and similar cases without side dielectric walls, are considered. Maximum errors are 1.4% for diagonal and 8.1% for off-diagonal values. Then, the same three strips of various positions in a two-layer dielectric medium are considered [16]. The comparison of the results obtained with TALGAT and those obtained using the integral equation method showed a maximum error of 8.8% for C entries and 0.8% for L entries.

The calculation of the capacitive matrices is carried out on the basis of solving a system of linear algebraic equations (SLAE). Analytical expressions for the elements of the SLAE matrix and the order of their calculation are described in [10], and are not given here.

The theoretical bases and algorithms for calculating quasistatic responses along each conductor of each multiconductor transmission line (MCTL) section interconnected to the total network were developed earlier and presented in [17]. The same algorithm is applicable for calculating simpler structures, for example, those considered in this work. Finally, there exist indicative and commonly available examples comparing the TALGAT software results with the measurement and electrodynamics analysis results, which are omitted here [11,18-21].

IV. SIMULATION RESULTS

Fig. 1–6 shows the cross-sections and connection diagram of the MFs under investigation. The simulation was performed with t = 70 μm, h

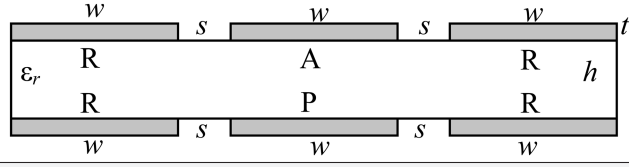

Fig. 1. MF cross-section with the conductors: R – reference, A – active, P – passive.

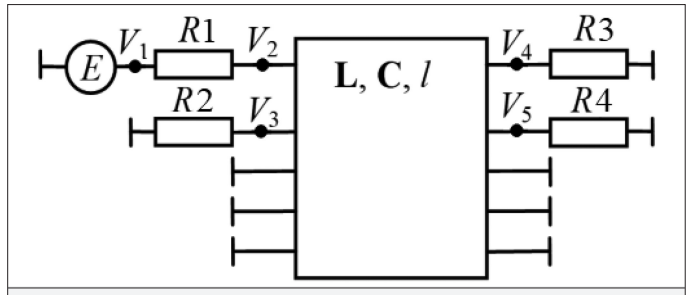

Fig. 2. MF connection diagram with all reference conductors.

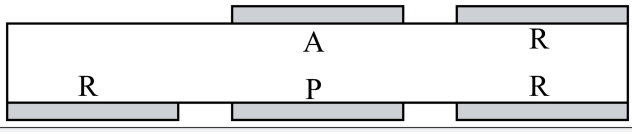

Fig. 3. Cross-section of the MF without upper-left reference conductor.

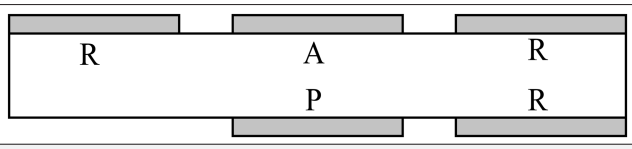

Fig. 4. Cross-section of the MF without upper and lower-left reference conductors.

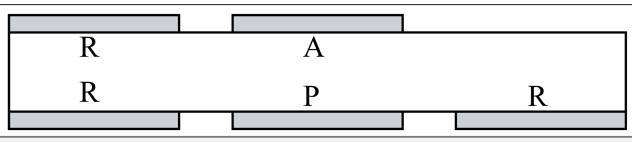

Fig. 5. Cross-section of the MF without upper-right reference conductor.

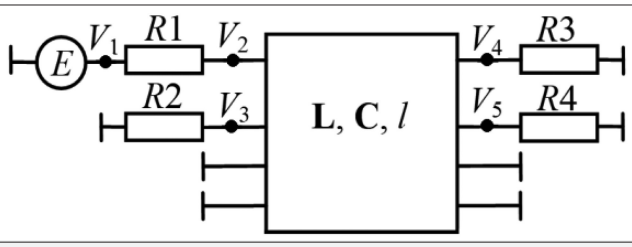

Fig. 6. MF connection diagram with reference conductors.

= 0.5 mm, w = 1 mm, s = 0.3 mm, $R1 = R2 = R3 = R4 = 50\ \Omega$, and the MF length ($l$) of 7 m. The greater length was chosen to eliminate the situation where APs overlap and complicate the process of determining their delays and calculating their possible combinations. The MF was excited with a single pulse with an amplitude of 2 V and a total duration of 150 ps. In the simulation process, the losses in dielectrics and conductors were not taken into account.

For accurate results, the matrix simulation should consider cross-section segmentation of the boundaries between conductors and dielectrics. For example, the sparse segmentation leads to inaccurate results. Therefore, a preliminary simulation was carried out with an increase in segmentation. It was taken uniform at all boundaries, but was controlled by the number of segments (n) at conductor edges (from 1 to 7). Its effect on mode delays and pulse amplitude at the MF output was estimated. The absence of significant changes in the results showed their convergence. The case was simulated when the MF had all the reference conductors.

Fig. 7 shows an example of the calculated time responses for different values of n. The per-unit-length delays and pulse amplitudes of the modes for all n are given in Table I. It can be seen that the small n value affects not only the per-unit-length delays but also the amplitude of the pulses. Thus, the maximum deviation of mode delays is observed for mode 2 (τ_2), and amplitudes for mode 3 (U_3). Therefore, the errors for these two parameters are given. The deviation of τ_2 is 1.5% for n = 1 and n = 3, 0.19% for n = 3 and n = 5, and 0.11% for n = 5 and n = 7. The deviation of pulse amplitudes is 2.4% for n = 1 and n = 3, 2.1% for n = 3 and n = 5, and 0% for n = 5 and n =7. It can be seen that when segmentation increases, the error becomes smaller. This is also confirmed by Fig. 7, which illustrates that at n = 5 and n = 7, the pulses overlap. This proves the convergence of the results. To save time, in further simulation, n is taken to be 5.

The correct calculation of the time response depends on two parameters: the time step or the number of counts (time discretes) to the front, and the number of counts for the pulse repetition period. When the time step is small, the Gibbs phenomenon can be observed. To exclude it, the time step was set to 5 ps, which is 10 counts to the front. A small number of counts can lead to non-physical results in the form of distortions. In addition, you can see that the other mode pulses arrived earlier rather than later in time. This is confirmed by Fig. 8, which shows the waveform distortions at the MF output. Besides, in addition to the main mode pulses, other pulses are observed (e.g., two pulses of negative polarity are seen between τ_1 and τ_2). Therefore, a preliminary simulation was performed with an increase in the number of counts for a period from 12 to 20. Fig. 8–11 show the simulation results at the MF output for different counts. The simulation results show that as the number of counts increases, the distortions get fewer. Thus, no distortions are observed at 18 counts (the Gibbs phenomenon is also not observed). This allows us to conclude that the results are correct. Therefore, further calculations were carried out at 18 counts.

The influence of the reference conductors on the per-unit-length mode delays and pulse amplitudes was described in [14]. Therefore, only APs are analyzed here.

Fig. 12 shows the simulation results at the MF output with a single pass of the mode pulses over the line, and Fig. 13 with a triple pass.

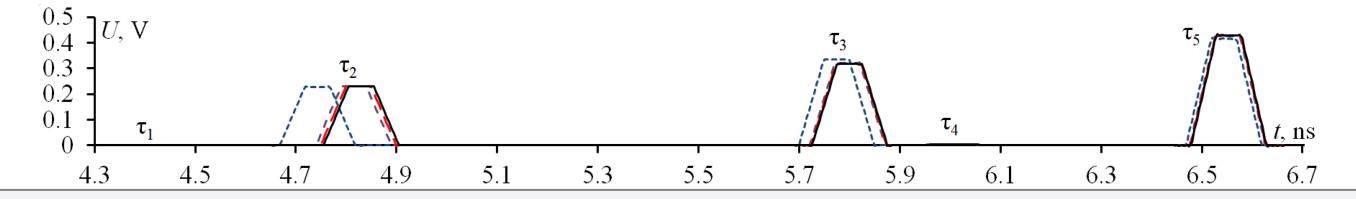

Fig. 7. Voltage waveforms at the MF output for n = 1 (- -), 3 (– –), 5 (–– ––), and 7 (–).

TABLE I. PER-UNIT-LENGTH MODE DELAYS (NS/M) AND PULSE AMPLITUDES (V) AT THE MF OUTPUT AT DIFFERENT VALUES OF *N*

N	τ_1	τ_2	τ_3	τ_4	τ_5	U_2	U_3	U_3	U_5
1	4.28691	4.66806	5.69942	5.92805	6.46844	0.228	0.335	0.0047	0.416
3	4.3484	4.74032	5.72099	5.93209	6.47563	0.230	0.327	0.0051	0.426
5	4.35586	4.74943	5.72346	5.9318	6.47681	0.230	0.320	0.0051	0.428
7	4.35996	4.75497	5.72532	5.93229	6.47818	0.230	0.320	0.0051	0.428

MF, modal filter.

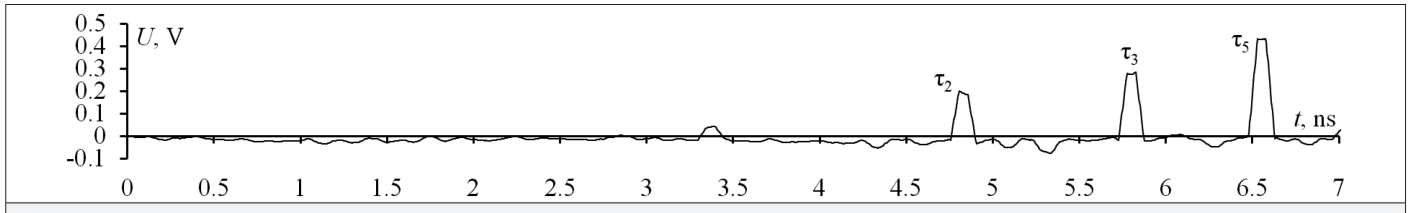

Fig. 8. Voltage waveforms at the MF output for 12 counts.

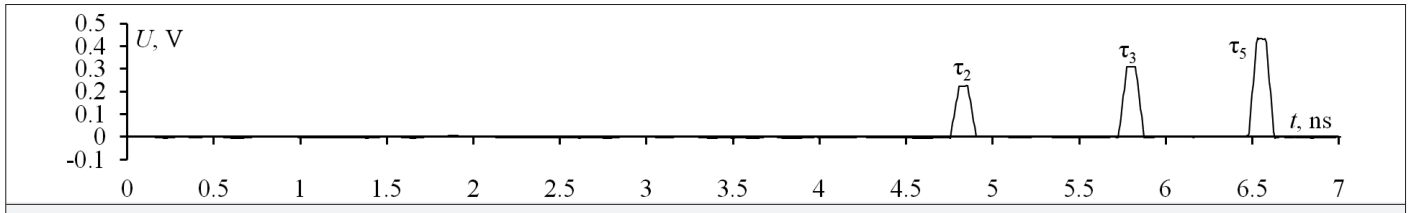

Fig. 9. Voltage waveforms at the MF output for 14 counts.

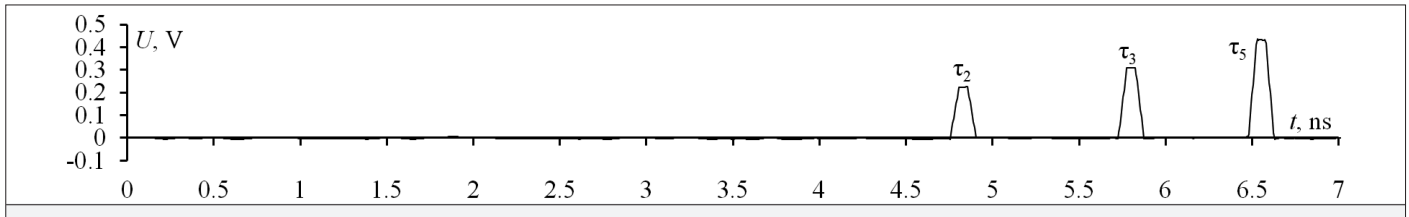

Fig. 10. Voltage waveforms at the MF output for 16 counts.

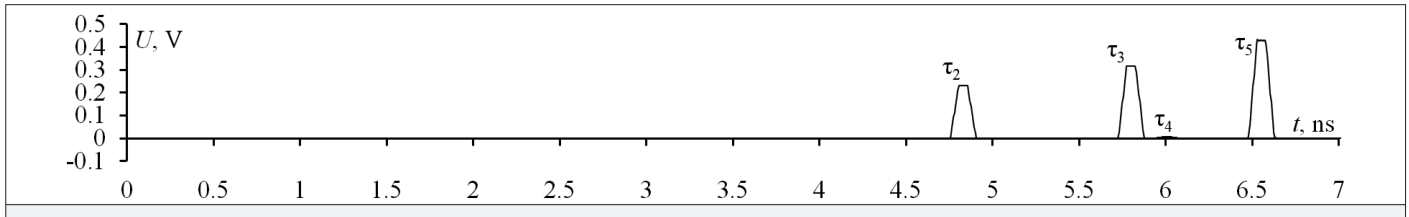

Fig. 11. Voltage waveforms at the MF output for 18 counts.

Table II shows the values of the per-unit-length delays and arrival times of the modes. Thus, there are no APs between the 5 pulses with one pass along the line, whereas, with a triple pass and further, they appear. At the output of the MF between time moments $/3\tau_1$ and $/3\tau_2$, there are two Aps; between $/3\tau_2$ and $/3\tau_3$, there are 18; between $/3\tau_3$ and $/3\tau_4$, it is 4; and between $/3\tau_4$ and $/3\tau_5$, it is 5.

As can be seen from Table III, the AP delays are determined by a linear combination of per-unit-length delays multiplied by the line length. Fig. 13 shows that the amplitude of some APs is greater than the amplitude of the mode pulses with triple pass through the line. Thus, for instance, AP 19 has a positive polarity and the amplitude of 0.155 V, while the amplitude of the second mode

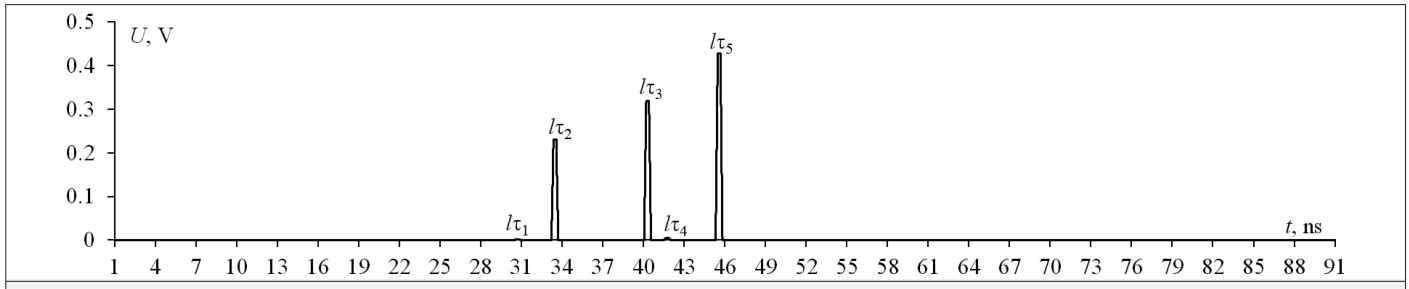

Fig. 12. Voltage waveforms at the MF output with a single pass of the mode pulses over the line.

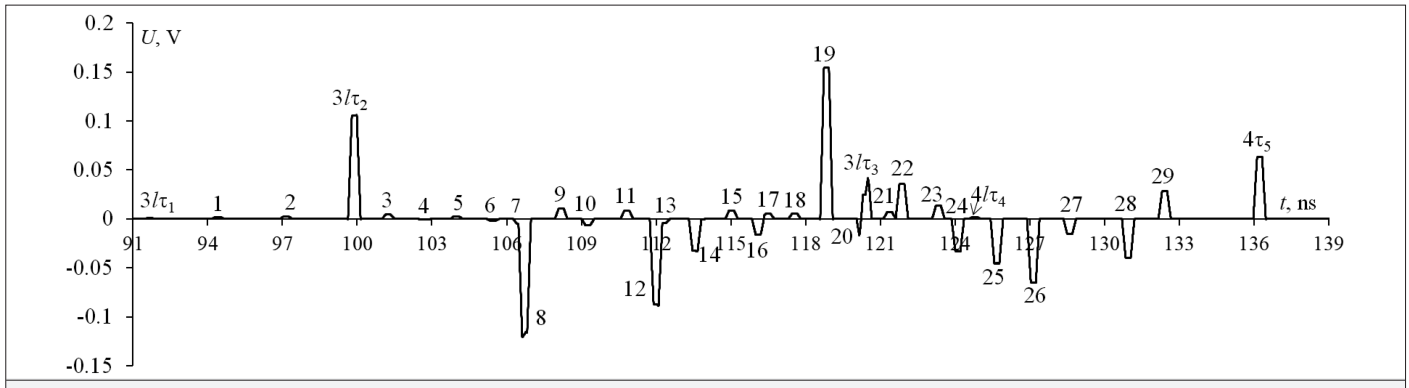

Fig. 13. Voltage waveforms at the MF output with a triple pass of the mode pulses over the line.

TABLE II. PER-UNIT-LENGTH MODE DELAYS (NS/M) AND MODE ARRIVAL TIMES (NS) FOR MF FROM FIG. 13.

τ_1	τ_2	τ_3	τ_4	τ_5	$l\tau_1$	$l\tau_2$	$l\tau_3$	$l\tau_4$	$l\tau_5$	$l3\tau_1$	$l3\tau_2$	$l3\tau_3$	$l3\tau_4$	$l3\tau_5$
4.35	4.74	5.72	5.93	6.47	30.47	33.21	40.05	41.51	45.32	91.41	99.63	120.15	124.54	135.971

MF, modal filter.

($3\tau_2$) is 0.105 V. The amplitude of AP 8 has negative polarity and the amplitude of 0.118 V. Table III shows the resulting combinations and the times of APs 1–29. As can be seen, the AP delays are determined by a linear combination of per-unit-length delays multiplied by the line length.

Fig. 14 and 15 show the simulation results at the MF output with the reference conductors removed. With the removal of one reference conductor (upper or lower), the input pulse is decomposed into 4 mode pulses. Table IV shows the values of the per-unit-length delays and arrival times of the modes for each of the MFs. Table V shows the results for APs 1–16. Fig. 15 shows that the polarity of APs 1 and 2 becomes negative. In the three MF configurations, the number and resulting combinations of APs are the same. The AP delays are determined by a linear combination of the per-unit-length delays of the line multiplied by its length. As can be seen from Fig. 15, the removal of the reference conductors influences not only the number of APs, but also their polarity and amplitude. For example, if the MF has all conductors, there are 29 APs; but when a conductor is removed, there are 16 APs. At the output of the MF between time moments $l3\tau_1$ and $l3\tau_2$, there are two APs; between $l3\tau_2$ and $l3\tau_3$, their number is 11; and between $l3\tau_3$ and $l3\tau_4$, there are 3. In the MF with all reference conductors, APs 1 and 2 have positive polarity and a small amplitude, but with the removal of the conductor, they change the polarity to negative and the amplitude becomes larger. As in the MF with all conductors, the removal of one reference conductor results in a greater amplitude of additional pulses than the pulse amplitude with the triple-mode pass. Therefore, for example, when the lower-left reference conductor is removed, AP 8 has the maximum amplitude, which is 0.128 V, while the amplitude of the second pulse with a triple pass along the line ($3l\tau_2$) is 0.121 V. With the removal of the upper-left reference conductor, all APs are less than triple-line pass mode pulses. However, AP 8 and the second pulse with triple pass have almost equal amplitudes of 0.086 V and 0.08 V, respectively. When the upper-right reference conductor is removed, AP 15 has maximum and negative polarity. Thus, the amplitude of the pulse 15 is 0.090 V, and the third mode with a triple pass ($3l\tau_3$) has the amplitude 0.055 V.

As can be seen from the results, each of the considered structures (except MF without upper-right reference conductor) has APs of amplitudes greater than the amplitude of a mode pulse with triple pass. This is important because when optimizing each of the structures or changing the boundary conditions at the ends of the passive conductor (short circuit (SC) – open circuit (OC) and OC – SC), the

TABLE III. ARRIVAL TIMES FOR APS (NS)

1	2	3	4	5	6	7	8	9	10	11	12	13	14	15	16	17	18	19	20	21	22	23	24	25	26	27	28	29
$l(2\tau_1+\tau_2)$	$l(\tau_1+2\tau_2)$	$l(2\tau_1+\tau_3)$	$l(2\tau_1+\tau_4)$	$l(\tau_1+\tau_2+\tau_3)$	$l(\tau_1+\tau_2+\tau_4)$	$l(\tau_3+2\tau_1)$	$l(2\tau_2+\tau_3)$	$l(2\tau_2+\tau_4)$	$l(\tau_1+\tau_2+\tau_3)$	$l(\tau_1+2\tau_3)$	$l(\tau_3+2\tau_2)$	$l(\tau_1+\tau_3+\tau_4)$	$l(\tau_2+2\tau_3)$	$l(\tau_2+\tau_3+\tau_4)$	$l(\tau_1+\tau_3+\tau_3)$	$l(\tau_2+2\tau_4)$	$l(\tau_1+\tau_4+\tau_3)$	$l(\tau_2+\tau_3+\tau_3)$	$l(\tau_2+\tau_4+\tau_3)$	$l(2\tau_3+\tau_1)$	$l(2\tau_3+\tau_4)$	$l(2\tau_4+\tau_3)$	$l(2\tau_3+\tau_2)$	$l(\tau_3+2\tau_3)$	$l(\tau_3+\tau_4+\tau_3)$	$l(\tau_3+2\tau_4)$	$l(2\tau_3+\tau_3)$	$l(2\tau_3+\tau_4)$
94.153	96.893	100.993	102.457	103.733	105.196	106.26	106.47	107.93	109.00	110.57	111.74	112.03	113.31	114.778	115.846	116.239	117.309	118.586	120.049	121.119	121.616	123.080	123.858	125.426	126.889	128.352	130.698	132.162

APs, additional pulses.

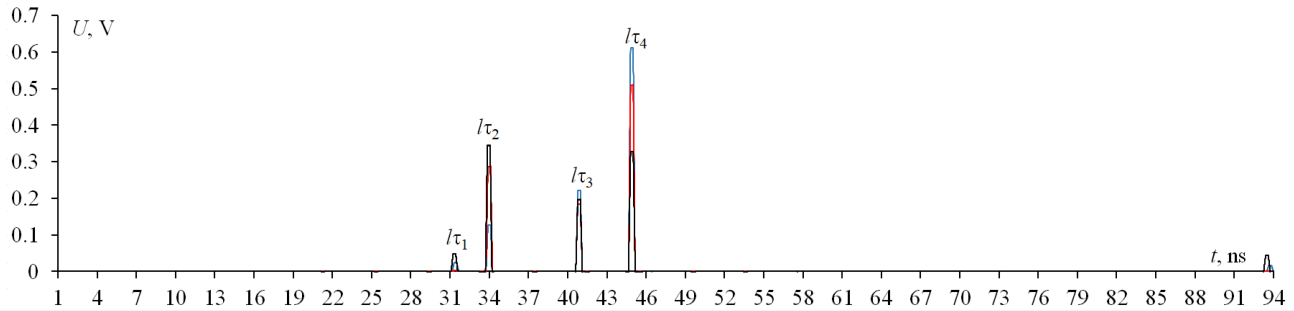

Fig. 14. Voltage waveforms at the output of MF without (–upper-left, –lower-left, and –upper-right) reference conductors with a single pass of the mode pulses along the line.

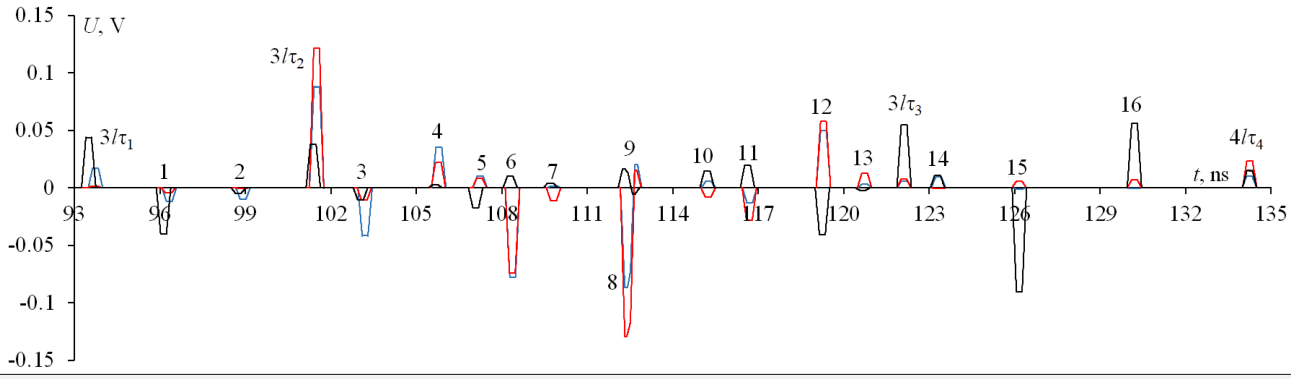

Fig. 15. Voltage waveforms at the output of MF without (–upper-left, –lower-left, and –upper-right) reference conductors with a triple pass of the mode pulses along the line.

TABLE IV. PER-UNIT-LENGTH MODES DELAYS (NS/M) FOR MF FROM FIG. 3 TO 5.

MF Without the Reference Conductor	τ_1	τ_2	τ_3	τ_4
Upper-right	4.440	4.816	5.803	6.380
Upper-left	4.452	4.822	5.803	6.380
Lower-left	4.450	4.821	5.803	6.380

MF, modal filter.

TABLE V. ARRIVAL TIME FOR APS (NS)

		MF Without a Reference Conductor		
No.	**Combination**	**Upper-Left**	**Lower-Left**	**Upper-Right**
1	$l(2\tau_1+\tau_2)$	96.08	96.05	95.87
2	$l(\tau_1+2\tau_2)$	98.67	98.65	98.50
3	$l(2\tau_1+\tau_3)$	102.95	102.92	102.80
4	$l(\tau_1+\tau_2+\tau_3)$	105.54	105.52	105.43
5	$l(2\tau_1+\tau_4)$	106.98	106.96	106.80
6	$l(2\tau_2+\tau_3)$	108.13	108.16	108
7	$l(\tau_1+\tau_2+\tau_4)$	109.57	109.56	109.5
8	$l(2\tau_2+\tau_4)$	112.16	112.16	112.08
9	$l(\tau_1+2\tau_3)$	112.41	112.39	112.32
10	$l(\tau_2+2\tau_3)$	115	114.99	114.95
11	$l(\tau_1+\tau_4+\tau_3)$	116.45	116.43	116.37
12	$l(\tau_2+\tau_3+\tau_4)$	119.03	119.03	118.99
13	$l(2\tau_4+\tau_1)$	120.48	120.48	120.41
14	$l(2\tau_4+\tau_2)$	123.07	123.08	123.03
15	$l(2\tau_3+\tau_4)$	125.91	125.90	125.91
16	$l(2\tau_4+\tau_3)$	129.94	129.95	130

APs, additional pulses; MF, modal filter.

amplitude of the main mode pulses will be less, due to which, a case is possible when the amplitude of APs will be greater.

V. CONCLUSION

Thus, the article investigates the appearance of APs in the time response of the MF implemented on a double-sided printed circuit board, as well as the ones with a reference conductor removed. The authors showed that APs appear in all of the presented MF structures. The delays of APs are determined by a linear combination of the per-unit-length delays of the line multiplied by its length.

In future, it is relevant to study the APs for situations when the boundary conditions at the ends of the passive conductor in all of the proposed MF structures change. This is important because in some MFs with the change of boundary conditions at the ends of the passive conductor, the amplitude of the APs is greater than the amplitude of the major modes. For example, this is observed in the MF with a passive conductor in the cutout of the reference plane.

Peer-review: Externally peer-reviewed.

Author Contributions: Concept – M.A.S.; Design – T.R.G.; Supervision – T.R.G.; Materials – M.A.S.; Data Collection and/or Processing – M.A.S.; Analysis and/or Interpretation – T.R.G.; Literature Search – M.A.S.; Writing Manuscript – M.A.S.; Critical Review – T.R.G.

Conflict of Interest: The authors have no conflicts of interest to declare.

Financial Disclosure: The research was supported by the Ministry of Science and Higher Education of the Russian Federation (Project FEWM-2020-0041) in TUSUR.

REFERENCES

1. Z. M. Gizatullin and R. M. Gizatullin, "Investigation of the immunity of computer equipment to the power-line electromagnetic interference," *J. Commun. Technol. Electron.*, vol. 61, no. 5, pp. 546–550, 2016. [CrossRef]
2. N. Mora, F. Vega, G. Lugrin, F. Rachidi, and M. Rubinstein, "Study and classification of potential IEMI sources," *Syst. Design Assess. Notes*, vol. 41, p. 91, 2014.
3. T. Weber, R. Krzikalla, J. L. TerHaseborg, and F. Sabath,"Linear and nonlinear filters suppressing UWB pulses,"*IEEE Trans. Electromagn. Compat.*, vol. 46, no. 3, pp. 423–430, 2004. [CrossRef]
4. C. Mojert, "UWB and EMP susceptibility of microprocessors and networks," in 14th International Zürich Symposium & Technical Exhibition on Electromagnetic Compatibility, Zurich, Switzerland, 2001, pp. 47–52.
5. Y. Zhao, G. Zhang, R. Guo, and F. Yang, "The breakdown characteristics of thermostable insulation materials under high-frequency square waveform," *IEEE Trans. Dielectrics Electr. Insul.*, vol. 26, no. 4, pp. 1073–1080, 2019. [CrossRef]
6. M. S. Nikoo, S. M.-A. Hashemi, and F. Farzaneh, "A two-stage DSRD-based high-power nanosecond pulse generator," *IEEE Trans. Plasma Sci.*, vol. 46, no. 2, pp. 427–433, 2018. [CrossRef]
7. X. C. Wang, Y. Y. Sun, J. H. Zhu, Y. H. Lou, and W. Z. Lu, "Folded feedthrough multilayer ceramic capacitor EMI filter, " *IEEE Trans. Electromagn. Compat.*, vol. 59, no. 3, pp. 996–999, 2017. [CrossRef]
8. D. Mansson and R. Thottappillil, "Comments on linear and nonlinear filters suppressing UWB pulses," *IEEE Trans. Electromagn. Compat.*, vol. 47, no. 3, pp. 671–672, 2005. [CrossRef]
9. A. T. Gazizov, A. M. Zabolotsky, and T. R. Gazizov, "UWB pulse decomposition in simple printed structures," *IEEE Trans. Electromagn. Compat.*, vol. 58, no. 4, pp. 1136–1142, 2016. [CrossRef]
10. A. M. Zabolotsky and T. R. Gazizov, "Experimental results on UWB pulse propagation in low-voltage power cables with different cross sections," *IEEE Trans. Electromag. Compat.*, vol. 54, no. 1, pp. 229–231, 2012. [CrossRef]
11. R. S. Surovtsev, A. V. Nosov, A. M. Zabolotsky, and T. R. Gazizov, "Possibility of protection against UWB pulses based on a turn of a meander microstrip line," *IEEE Trans. Electromagn. Compat.*, vol. 59, no. 6, pp. 1864–1871, 2017. [CrossRef]
12. A. O. Belousov *et al.*, "From symmetry to asymmetry: The use of additional pulses to improve protection against ultrashort pulses based on modal filtration," *Symmetry*, vol. 12, no. 7, p. 1117, 2020. [CrossRef]
13. M. A. Samoylichenko and T. R. Gazizov, "Parametric and structural optimization of the modal filter on a double-sided printed circuit board," *J. Phys. Conf. S.*, vol. 1862, no. 1, pp. 1–7, 2021. [CrossRef]
14. T. R. Gazizov, I. Y. Sagiyeva, and S. P. Kuksenko, "Solving the complexity problem in the electronics production process by reducing the sensitivity of transmission line characteristics to their parameter variations," *Complexity*, vol. 2019, no. 6301326, pp. 1–11, 2019.
15. J. Venkataraman, S. M. Rao, A. R. Djordjevic, T. K. Sarkar, and Y. Naiheng, "Analysis of arbitrarily oriented microstrip transmission lines in arbitrarily shaped dielectric media over a fnite ground plane," *IEEE Trans. Microw. Teory Tech.*, vol. MTT–33, no. 10, pp. 952–960, 1985.
16. W. Delbare and D.De Zutter, "Space-domain green's function approach to the capacitance calculation of multiconductor lines in multilayered dielectrics with improved surface charge modeling," *IEEE Trans. Microwave Theory Techn.*, vol. 37, no. 10, pp. 1562–1568, 1989. [CrossRef]
17. R. R. Gazizov, T. T. Gazizov, and T. R. Gaizov, "Detection and localization of interference and useful signal extreme points in closely coupled multiconductor transmission line networks," *Symmetry*, vol. 11, no. 10, pp. 1–33, 2019. [CrossRef]
18. A. T. Gazizov, A. M. Zabolotskii, and T. R. Gazizov, "Measurement and simulation of time response of printed modal filters with broad-side coupling," *J. Commun. Technol. Electron.*, vol. 63, no. 3, pp. 270–276, 2018. [CrossRef]
19. P. E. Orlov, T. R. Gazizov, and A. M. Zabolotsky, "Short pulse propagation along microstrip meander delay lines with design constraints: Comparative analysis of the quasi-static and electromagnetic approaches," *Appl. Comp. Electromagn. Soc. J.*, vol. 31, no. 3, pp. 238–243, 2016
20. M. A. Samoylichenko, Y. S. Zhechev, V. P. Kosteletskii, and T. R. Gazizov, "Electrical characteristics of a modal filter with a passive conductor in the reference plane cutout," *IEEE Trans. Electromagn. Compat.*, vol. 63, no. 2, pp. 435–442, 2020. [CrossRef]
21. E. B. Chernikova, A. O. Belousov, T. R. Gazizov, and A. M. Zabolotsky, "Using reflection symmetry to improve the protection of radio-electronic equipment from ultrashort pulses," *Symmetry*, vol. 11, no. 7, 2019. [CrossRef]

Maria A. Samoylichnko was born in Temirtau, Kazakhstan in 1993. Received the BSc and MSc degrees in Engineering from Tomsk State University of Control Systems and Radioelectronics (TUSUR) in 2015 and 2017, respectively. Currently, he is a postgraduate student and also works as a Junior Researcher at TUSUR. She is the author and coauthor of 18 scientific papers.

Talgat R. Gazizov was born in 1963. He received the Engineering degree, the Ph.D. degree, and the Dr. habil. of Engineering Sciences degree from Tomsk State University of Control Systems and Radioelectronics (TUSUR), Tomsk, Russia, in 1985, 1999, and 2010, respectively. His current research interests includes signal integrity problem. He is the author or coauthor of 388 scientific papers.